

**Nontrivial effect of spin-orbit coupling on the intrinsic resistivity of ferromagnetic gadolinium**Mingfeng Zhu, Haibo Yao, Liwei Jiang , and Yisong Zheng \**Key Laboratory of Physics and Technology for Advanced Batteries (Ministry of Education), College of Physics, Jilin University, Changchun 130012, China*

(Received 8 November 2022; revised 28 January 2023; accepted 18 February 2023; published 1 March 2023)

As a metallic material of a heavy atom, elemental gadolinium (Gd) has many extraordinary electronic properties associated with the strong correlation and spin-orbital coupling (SOC). Previous studies have shown that the resistivity of ferromagnetic (FM) Gd due to the spin fluctuation scattering is comparable to the intrinsic resistivity limited by electron-phonon (e-ph) scattering even near the room temperature. However, such theoretical explanations cannot account for the experimental observation quantitatively. In the present work, by performing the first-principles calculations, we find that the intrinsic resistivity is insensitive to Hubbard  $U$ , i.e., the electronic correlation. On the contrary, when the effect of SOC is taken into account, the band structure near the Fermi level is modified greatly. As a result, the calculated intrinsic resistivity increases by nearly 3 times over that without SOC. By further counting in the additional resistivity contributed from spin fluctuation scattering, our theoretical result of resistivity agrees very well with the experimental observation of resistivity of FM Gd as a function of temperature.

DOI: [10.1103/PhysRevB.107.115101](https://doi.org/10.1103/PhysRevB.107.115101)**I. INTRODUCTION**

Materials with heavy elements, especially the transition metallic atoms and rare-earth atoms, are characterized by the strong electronic correlation and spin-orbital coupling (SOC). A variety of significant physical phenomena such as the magnetism, high-temperature superconductivity, Kondo effect, and Mott transition can often be observed in such materials [1–3], most of which are attributed to the strong correlation effect introduced by the  $d$  or  $f$  orbitals of heavy atoms. In addition, the strong SOC of heavy atoms can bring about the band inversion, hence resulting in the topological transition [4]. Thus far, many topological nontrivial materials involve heavy elements. As such, one can say that heavy elements often play a crucial role for determining the extraordinary electronic properties of materials.

As a representative of lanthanide materials, elemental gadolinium (Gd) in its single-crystal form is a ferromagnetic (FM) metallic material with partially occupied  $4f$  and  $5d$  bands at temperature lower than the Curie temperature. Therefore, it is a correlated electron system and also has strong SOC. Research on Gd has a long history [5]. Nonetheless, it has never ceased to get attention since interesting experimental observations about various physical properties were reported successively on such an elemental metal [6–13]. For example, very recently, Gd has been experimentally demonstrated to be a Dirac magnon material by inelastic neutron scattering, which draws much attention [14]. All of these experimental results on Gd call for reasonable theoretical explanations, preferably on the level of quantitative coinci-

dences with experimental results. However, because of the strong electronic correlation and SOC in Gd, it is not a simple task even to explain the experimental observations on some fundamental physical properties which can be well described within band theory in other conventional solids. For instance, to our knowledge, the theoretical result on the resistivity of FM Gd as a function of temperature is at odds with the relevant experimental measure [15]. In general, the resistivity of most metals around room temperature is dominated by the e-ph scattering which is called the intrinsic resistivity of metal since it is inevitable even in a perfect lattice. In contrast, the contributions of other scattering mechanisms to the resistivity are much smaller at room temperature. However, it is not such a case for Gd which has the FM phase as the ground state with a high Curie temperature of  $T_c = 293$  K [16], in the range of room temperature. Theoretical analysis indicated that the e-ph scattering limited intrinsic resistivity does not agree well with the measured resistivity of FM Gd even when the temperature is close to  $T_c$  [17]. Consequently, one must consider other possible scattering mechanisms, at least comparable to the effect of e-ph scattering. Previous theoretical studies suggested that the scattering due to spin fluctuation is as important as e-ph scattering near room temperature [18,19]. In relevant theoretical work, both kinds of resistivity limited by e-ph scattering and spin fluctuation of FM Gd were theoretically treated on the equal footing, by employing the so-called coherent potential approximation (CPA). Usually, CPA is believed to be a successful approximation to deal with spin fluctuation, impurity, and disorder scatterings. However, as a quasistatic theory, CPA disregards the inelastic nature of e-ph scattering. Furthermore, it has to use an empirical model to estimate the Debye frequency [20,21]. Therefore, the approach using CPA is not a fully first-principles calculation on the intrinsic resistivity of materials, such as Gd. Just owing to these draw-

\*zhengys@jlu.edu.cn

backs, in the previous work the calculated resistivity of Gd with both the e-ph and spin fluctuation scatterings taken into account is still not satisfactory, which cannot account for the experimental result quantitatively.

Thus far, it is not difficult to calculate the electronic band energy of most realistic materials within the theoretical framework of the density functional theory (DFT). Besides, the phonon frequency and the e-ph interaction matrix elements can also be obtained by means of the density functional perturbation theory (DFPT) [22] or the so-called frozen-phonon method. More importantly, the effects of electronic correlation and SOC on the electronic states, the phonon frequency, as well as the e-ph interaction are incorporated into the calculations by using the DFT+ $U$  [23–26] and DFPT+ $U$  [27,28] methods and by choosing appropriate relativistic pseudopotential. This theoretical progress paves the way for explaining or predicting the experimental observation of electronic transport property of actual materials. In such a context, it is now feasible to revisit the issue of the intrinsic resistivity of Gd on the level of the first-principles calculations, with the purpose to explain the relevant experimental observations quantitatively.

In this paper, within the theoretical framework of DFT+ $U$  and DFPT+ $U$ , we calculate the electronic and phonon dispersion, together with the e-ph interaction matrix elements of Gd. Then, with these calculated quantities as the input to solve the Boltzmann transport equation (BTE) numerically, we can perform the *ab initio* study on the intrinsic resistivity of FM Gd. We find that the Hubbard  $U$  has very limited impact on the intrinsic resistivity of FM Gd. In contrast, due to the substantial modification to the band structure, the SOC effect increases the intrinsic resistivity by nearly 3 times over the one without SOC. As a result, after counting in the contribution of spin fluctuation scattering to the resistivity from Ref. [15], we obtain the final result of resistivity of FM Gd, agreeing with the experiment results quantitatively.

The rest of the present work is organized as follows. In Sec. II, we give the details of the parametric setup for first-principles calculations and the theoretical formulas to calculate the intrinsic resistivity of FM Gd. In Sec. III, we discuss the numerical results. In Sec. IV, the main conclusions are summarized.

## II. COMPUTATIONAL METHOD

In this paper, the collinear spin-polarized DFT+ $U$ , DFPT+ $U$ , and noncollinear DFT and DFPT calculations are performed by using the QUANTUM ESPRESSO (QE) package [29,30]. The norm-conserving pseudopotential with the local-density approximation (LDA) functional together with a 90 Ry kinetic energy cutoff is used. The Brillouin zone (BZ) of electronic states is sampled by a coarse Monkhorst-Pack mesh of  $12 \times 12 \times 12$ , whereas that of phonon states by a mesh of  $3 \times 3 \times 3$ . The resistivity is calculated on a much finer mesh on the BZ for both electrons and phonons in the framework of iterative linearized BTE [31–33] with the help of Wannier interpolation techniques as implemented in Wannier90 [34] and the PERTURBO code [35]. The convergences of conductivity or resistivity calculated throughout the paper are all tested.

The basic formulations for linearized BTE are as follows. The e-ph scattering limited conductivity driven by an electric field according to the linearized BTE has the form

$$\sigma = \frac{2e^2}{N_k \Omega k_B T} \sum_{nk} f_{nk}(1-f_{nk})(\mathbf{v}_{nk} \cdot \boldsymbol{\epsilon})(\mathbf{F}_{nk} \cdot \boldsymbol{\epsilon}), \quad (1)$$

where  $e$  is the elementary charge,  $k_B$  the Boltzmann constant, and  $T$  the temperature. The Fermi-Dirac distribution for the electron in states with band index being  $n$  and electron wave vector being  $\mathbf{k}$  is denoted by  $f_{nk}$ .  $\boldsymbol{\epsilon}$  is a unit vector pointing to the electric field direction.  $N_k$  is the number of the  $k$  points for sampling the BZ.  $\Omega$  is the unit cell volume.  $\mathbf{v}_{nk} = \nabla E_{nk}/\hbar$  is the electron velocity. The factor  $f_{nk}(1-f_{nk})$  as a function of the electronic energy  $E_{nk}$  has a sharp peak around Fermi energy. This feature implies that the intrinsic conductivity is dominated by the electron states around the Fermi level. In other words, the nearer the eigenenergy of the electron is to the Fermi level, the larger its contribution to the conductivity is. Because of this,  $f_{nk}(1-f_{nk})$  defines a temperature-smeared Fermi window relevant to the intrinsic conductivity (resistivity). The width of the Fermi window is on the scale of a couple of the thermal excitation energies. Throughout the paper, the Fermi window is set to be  $\pm 0.3$  eV around the Fermi level, which is wide enough for the convergence of the Fermi window related variables, such as the conductivity, in the temperature range we are interested in.

$\mathbf{F}_{nk}$  describes the mean-free path of the electron in state  $|nk\rangle$  limited by e-ph scattering and is

$$\mathbf{F}_{nk} = \mathbf{v}_{nk} \tau_{nk} + \tau_{nk} \sum_{mqv} (G_{nk,-qv}^{mk+q} + G_{nk,qv}^{mk+q}) \mathbf{F}_{mk+q} \quad (2)$$

with

$$G_{nk,-qv}^{mk+q} = \frac{2\pi}{\hbar} |g_{nk,qv}^{mk+q}|^2 (1 + N_{-qv} - f_{mk+q}) \times \delta(E_{nk} - \hbar\omega_{-qv} - E_{mk+q}) \quad (3)$$

and

$$G_{nk,qv}^{mk+q} = \frac{2\pi}{\hbar} |g_{nk,qv}^{mk+q}|^2 (N_{qv} + f_{mk+q}) \times \delta(E_{nk} + \hbar\omega_{qv} - E_{mk+q}), \quad (4)$$

where  $\mathbf{q}$  stands for phonon wave vector,  $\omega_{qv}$  phonon frequency,  $\nu$  phonon mode, and  $N_{qv}$  the phonon boson distribution function.  $g_{nk,qv}^{mk+q}$  is the e-ph interaction matrix element.  $\tau_{nk}$  is the relaxation time of electronic state  $|nk\rangle$  due to e-ph scattering, and its inverse is just the corresponding scattering rate which takes a form as

$$\frac{1}{\tau_{nk}} = \frac{2\pi}{\hbar} \sum_{mqv} |g_{nk,qv}^{mk+q}|^2 \times [(1 + N_{-qv} - f_{mk+q})\delta(E_{nk} - \hbar\omega_{-qv} - E_{mk+q}) + (N_{qv} + f_{mk+q})\delta(E_{nk} + \hbar\omega_{qv} - E_{mk+q})]. \quad (5)$$

With the calculated conductivity, the intrinsic resistivity can then be obtained by using

$$\rho = 1/\sigma. \quad (6)$$

If the second term in Eq. (2) is neglected, the formulas reduce to the ones in the energy relaxation time approximation

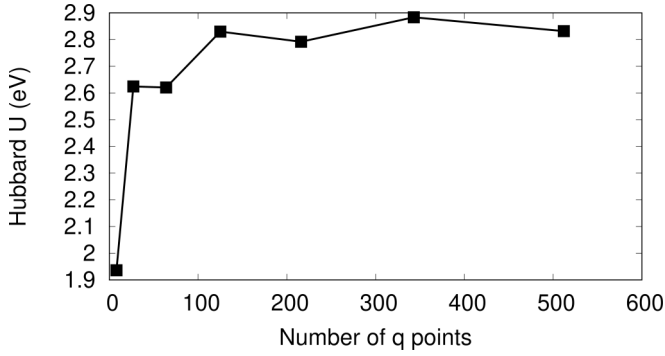


FIG. 1. The convergence test on the Hubbard  $U$  against the number of  $q$  points by using the linear response approach.

(ERTA) [31] which can be adopted to analyze the numerical results in the next section. In ERTA, the conductivity has the form of

$$\begin{aligned} \sigma &= \frac{2e^2}{N_k \Omega \hbar k_B T} \sum_{nk} f_{nk} (1 - f_{nk}) (v_{nk} \cdot \epsilon)^2 \tau_{nk} \\ &= \sum_{nk} \sigma_{nk}, \end{aligned} \quad (7)$$

where  $\sigma_{nk}$  is electronic state resolved conductivity.

### III. RESULTS AND DISCUSSION

Accordingly to previous experimental works [6,36], elemental Gd in its single-crystal form has the hexagonal close-packed structure with lattice constants of  $a_0 = 3.63 \text{ \AA}$  and  $c_0 = 5.78 \text{ \AA}$ . And the FM phase is the ground state with the Curie temperature  $T_c = 293 \text{ K}$  [16]. The measured magnetic moment per Gd atom is  $7.63 \pm 0.01 \mu_B$  [37]. Our numerical calculations can well reproduce these results. And in the following we will focus only on the intrinsic resistivity of single-crystal Gd in the FM ground state at a temperature lower than the Curie temperature.

#### A. The impacts of Hubbard $U$

To partially incorporate the electronic correlation effect into the mean-field theory, the DFT+ $U$  method is a widely adopted method on the level of the first-principles calculations for correlated electron systems, especially for lanthanide and actinide. The Hubbard  $U$  can be determined without any adjustable parameters within the linear response approach [38,39]. Here, by performing numerical calculation within the linear response approach, we find that the Hubbard  $U$  for FM Gd converges to 2.83 eV, as shown in Fig. 1. Besides, we further find that the calculated lattice constants and the magnetic moment per atom with  $U = 2.83 \text{ eV}$  deviate less than 0.5 percent from the ones with  $U = 0 \text{ eV}$ . This indicates

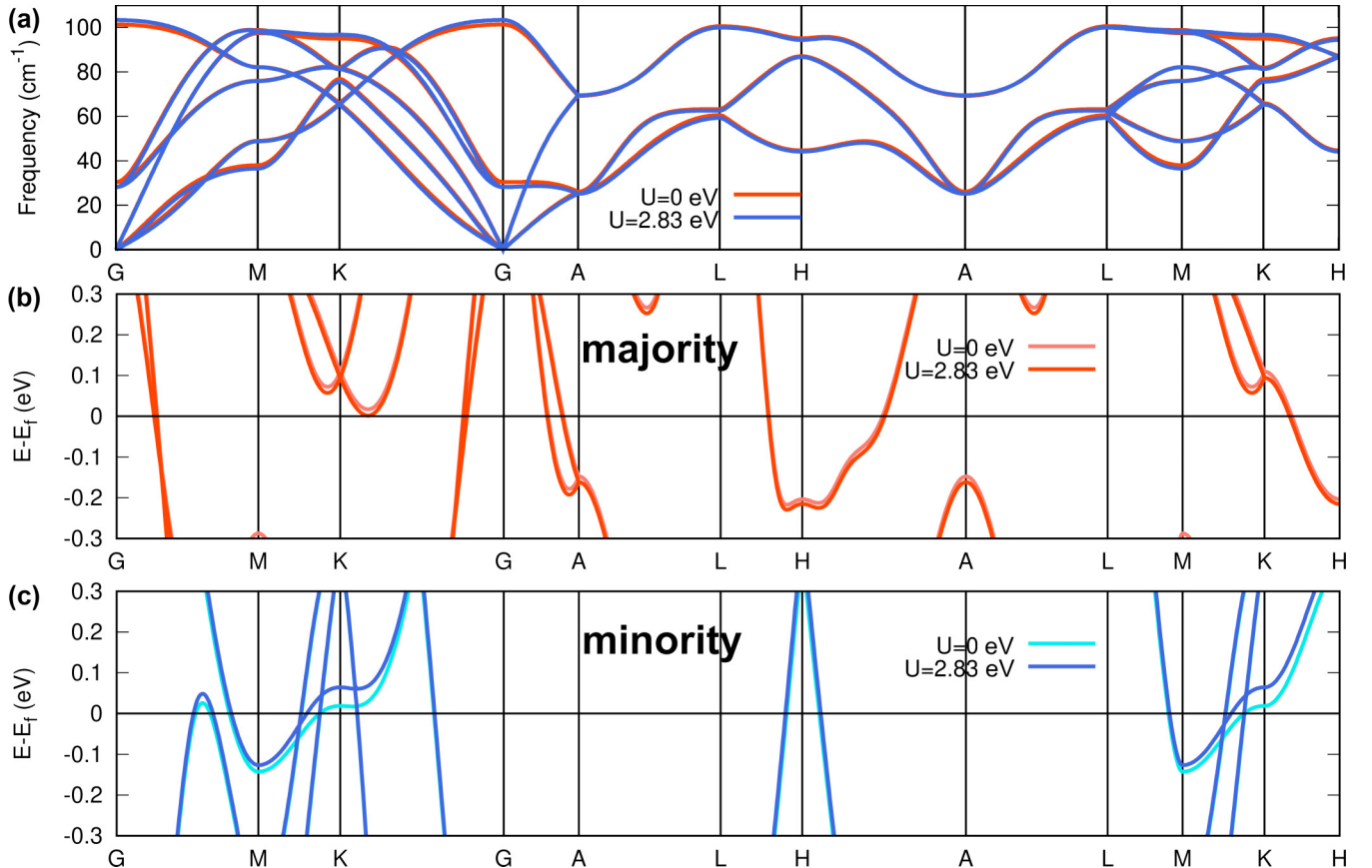


FIG. 2. (a) The phonon band structure of FM Gd with  $U = 0 \text{ eV}$  and  $U = 2.83 \text{ eV}$ . The spin-polarized electron band structures for electrons in (b) majority spin states and (c) minority spin states of ferromagnetic (FM) gadolinium (Gd) with  $U = 0 \text{ eV}$  and  $U = 2.83 \text{ eV}$ .

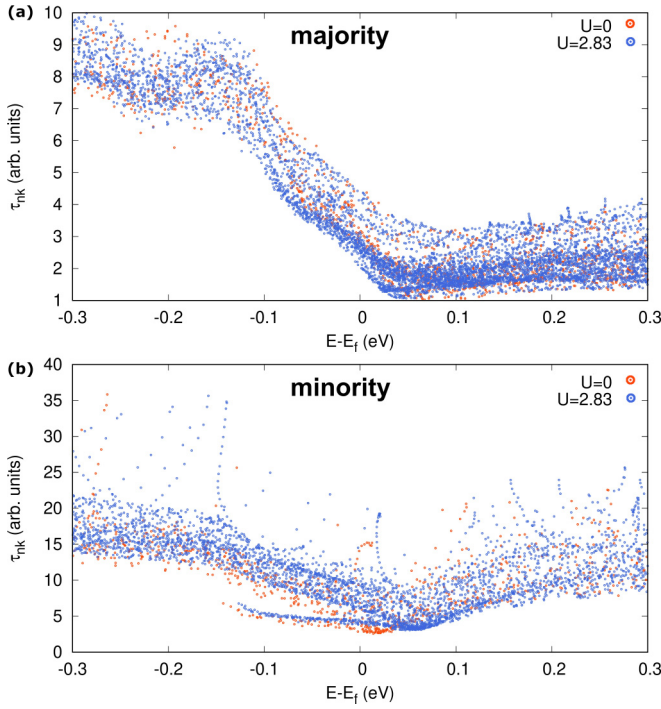


FIG. 3. The relaxation times  $\tau_{nk}$  for electrons in (a) majority spin states and (b) minority spin states near the Fermi level with  $U = 0$  eV and  $U = 2.83$  eV at 280 K.

that the Hubbard  $U$  has very limited impact on the crystal structure and magnetism of FM Gd.

The intrinsic resistivity or conductivity depends on the electronic band energy, phonon dispersion, and e-ph scattering rate. Therefore, in the following we study the impact of  $U$  on these relevant quantities respectively. As one can see from Fig. 2(a), the phonon band structure is affected insignificantly by  $U$ . Moreover, as shown in Figs. 2(b) and 2(c),  $U$  also has very limited impact on the electronic band structure of FM Gd near the Fermi level, especially for electrons in majority spin states. The major variation in the band structure happens near the high-symmetry point K where the electrons in minority spin states on the flat band near the Fermi level are raised by approximately 0.05 eV with respect to the Fermi level. Figure 3 shows the relaxation time  $\tau_{nk}$  defined by Eq. (5) at 280 K as a function of the eigenenergy  $E_{nk}$  relative to the Fermi energy  $E_f$ . Note that only those electron states  $|nk\rangle$  in the Fermi window are considered in the numerical results shown in Fig. 3 since only those states contribute to the intrinsic resistivity substantially. As one can see, the differences between the relaxation times for electrons in majority spin states with different  $U$  are insignificant, while the relaxation times increase slightly as  $U$  increases from 0 to 2.83 eV for electrons in minority spin states. This indicates that  $U$  increases the overall relaxation times of the electrons near the Fermi level and consequently increases the conductivity of FM Gd to a small extent.

Figure 4 shows the temperature dependence of the calculated resistivities along the  $x$  and  $z$  directions, i.e., the  $b$  axis and  $c$  axis of the hexagonal lattice, respectively. The appreciable difference of the intrinsic resistivities between the

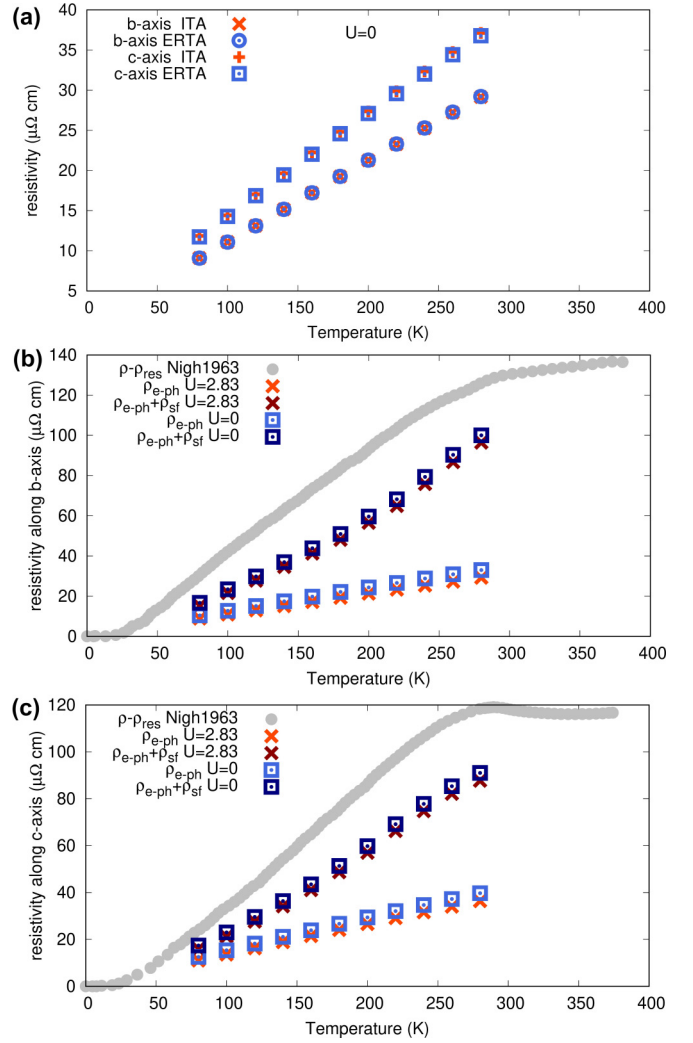


FIG. 4. (a) The calculated resistivity along  $x$  and  $z$  directions, i.e., the  $b$  axis and  $c$  axis of the hexagonal lattice, respectively. The Hubbard  $U$  is set to 0. ITA for resistivity calculated iteratively and ERTA for resistivity in energy relaxation time approximation (ERTA). The measured and calculated resistivities of FM Gd (b) along  $b$  axis and (c) along  $c$  axis as a function of temperature. The measured resistivity shown as the gray circles [16].  $\rho_{\text{e-ph}}$  stands for the intrinsic resistivity arisen from e-ph scattering and  $\rho_{\text{sf}}$  for the one limited by the spin fluctuation calculated in Ref. [15]. The calculated intrinsic resistivities are all in ERTA.

two distinct transport directions is due to the different Fermi velocities of electronic states in the two directions. In addition, those results of resistivity shown in Fig. 4 are obtained by using two kinds of numerical approaches, i.e., the iteration solution of the BTE and ERTA. We can see that the two kinds of numerical results agree with each other very well in the whole temperature range. This implies that the iteration process cannot bring about nontrivial change of the intrinsic resistivity, regardless of the electronic transport direction. As shown in Figs. 4(b) and 4(c), the intrinsic resistivity has only a trivial decrease when the Hubbard  $U$  takes a nonzero value, in comparison with the result of  $U = 0$  eV. This numerical result is consistent with the calculated relaxation time as shown in Fig. 3(b) which indicates that the relaxation time of minority

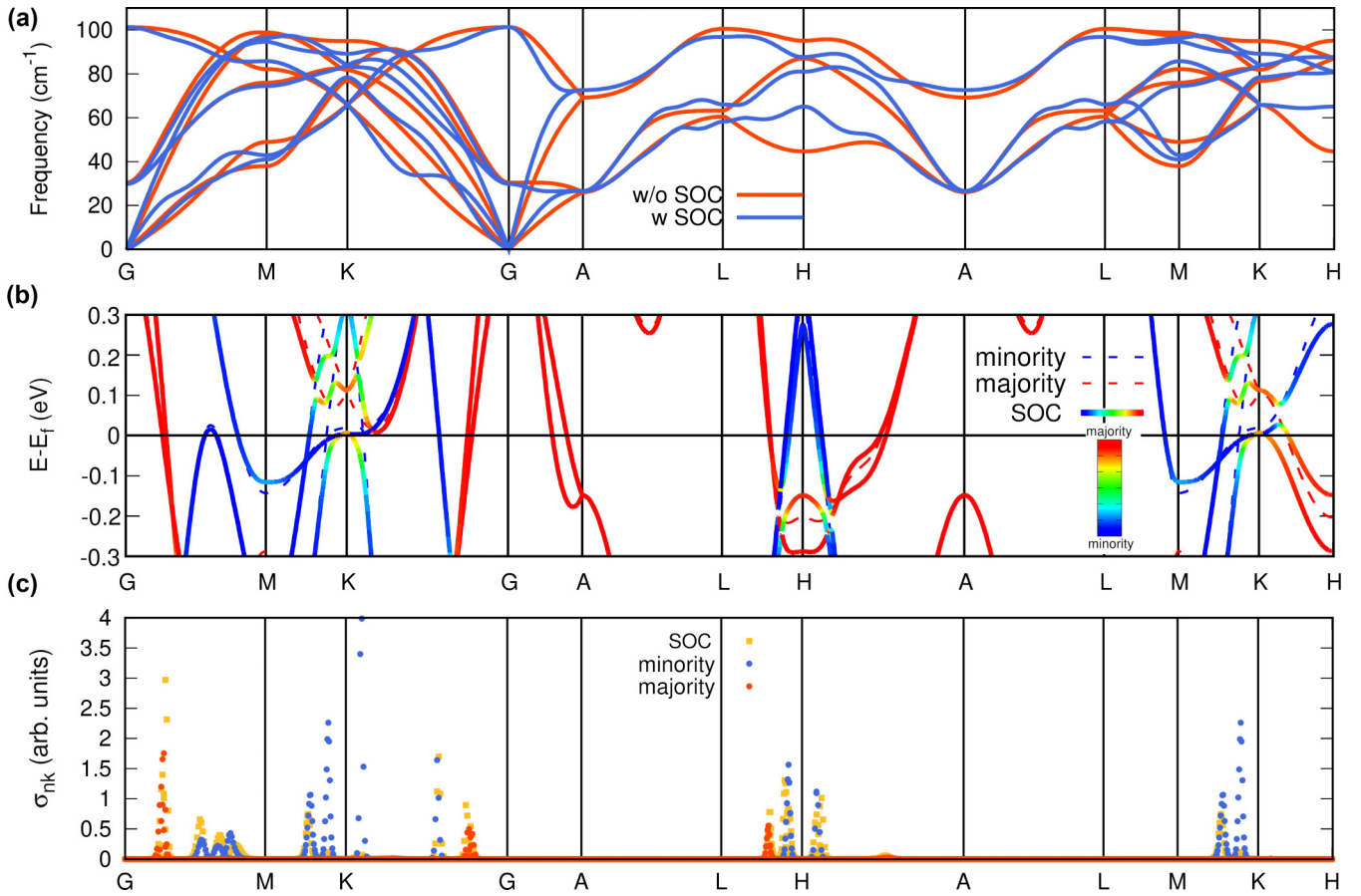


FIG. 5. (a) The phonon band structure of FM Gd with SOC and without SOC. (b) The electron band structures of FM Gd with SOC. The spin polarization along  $z$  axis is projected as shown in the color bar when considering SOC effect. The band structures without SOC are also plotted as red and blue dashed lines for majority spin states and minority states, respectively, as reference.  $E_f$  stands for the Fermi level. (c) The electronic state resolved conductivity  $\sigma_{nk}$ . And the driving electric field is along  $b$  axis at 280 K. Note that  $\sigma_{nk}$ 's are shown in an arbitrary units since only their relative values make sense for the discussion in the context.

spin states near the Fermi level is enhanced slightly by a nonzero  $U$  value. More importantly, it can be clearly found from Figs. 4(b) and 4(c) that the intrinsic resistivity is far lower than the experimental result of the resistivity even near the room temperature. When the resistivity due to the spin fluctuation is counted in, the theoretical result of the resistivity becomes closer to the experimental result in the total temperature range. But a nontrivial difference between them remains.

Considering that the value of the Hubbard  $U$  can be determined by other methods, we also perform numerical calculations similar to those of the aforementioned properties with other Hubbard- $U$  values. Specifically, we calculated and compared the crystal structures, magnetic moments per atom, electronic band structures near the Fermi level, phononic band structures, relaxation times, and resistivities of FM Gd with  $U = 0, 1, 2, 3, 4, 5,$  and  $6$  eV. The results are quite similar, without substantial differences. In other words, the Hubbard  $U$  has very limited impact on the above properties, especially on the intrinsic resistivity, our main concern.

### B. The impacts of SOC

Now that electronic correlation (Hubbard  $U$ ) does not affect the intrinsic resistivity of Gd notably, we turn to pay

attention to the effect of SOC on the intrinsic resistivity of Gd. To begin with, let us compare the phonon spectrum of FM Gd with and without SOC. The result is shown in Fig. 5(a). We find that SOC hardens slightly the low-frequency phonon around the  $\Gamma$  point, i.e., the BZ center. This result intends to lower the number of low-frequency acoustic phonons and hence to lower the possibility of e-ph scattering. According to this result and considering that the low-frequency phonons play the crucial role to affect the electronic transport, we can say that the SOC effect on phonon dispersion reduces slightly the intrinsic resistivity if the effect of SOC on phonon dispersion is exclusively taken into account. Obviously, this result is just opposite to the fact that theoretical result of resistivity is appreciably smaller than the experimental observation as shown in Fig. 4.

The electronic band structures of FM Gd with and without SOC effect are compared in Fig. 5(b). One can see that SOC modifies the band structure remarkably just around K and H points in the BZ. In contrast, in other regions of the BZ [not limited to the high-symmetry lines as shown in Fig. 5(b)], our numerical results indicate that the band structure does not change nontrivially by SOC. Considering that the band modification by SOC around the H point is far lower than the Fermi level, i.e., nearly outside the Fermi window, the

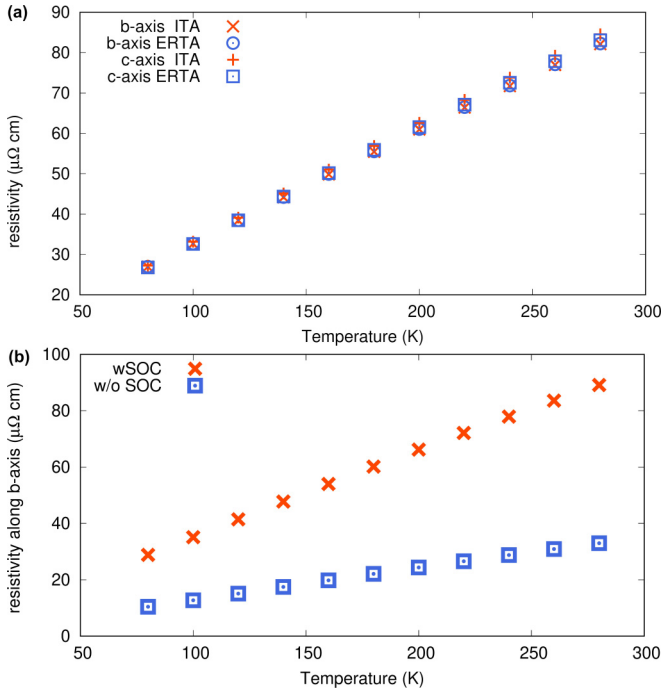


FIG. 6. (a) The calculated resistivity with SOC along  $b$  and  $c$  axes in ERTA and iteratively on a  $\mathbf{k}$  and  $\mathbf{q}$  mesh of  $30 \times 30 \times 30$ . (b) The calculated converged resistivity of FM Gd with SOC and without SOC along  $b$  axis on a finer  $\mathbf{k}$  and  $\mathbf{q}$  mesh of  $50 \times 50 \times 50$ .

electronic states therein cannot influence the intrinsic resistivity substantially. On the contrary, the band modification around the K point which is characterized by the opening of the band gap just appears around the Fermi level, falling in the Fermi window. From such a result one can infer reasonably that the SOC will give rise to a remarkable modification on the calculated intrinsic resistivity. Such a prediction is verified by the numerical result shown in Fig. 5(c) where the electronic state resolved resistivities, i.e.,  $\sigma_{nk}$  defined in Eq. (7) with the driving electric field being along the  $b$  axis, are displayed for those electronic states in the Fermi windows and along the same high-symmetry lines in the BZ with the plot of the band structure shown in Fig. 5(b). We can see that  $\sigma_{nk}$ 's around the K point decrease dramatically due to the nontrivial SOC effect on the band structure therein. In contrast, the  $\sigma_{nk}$ 's elsewhere in the BZ are not altered nontrivially by the SOC. Based on the numerical result shown in Fig. 5(c), we can expect a sizable increase of the intrinsic resistivity when the SOC effect on the band structure is incorporated into the calculations.

Similarly to the case without SOC, when SOC is taken into account, as shown in Fig. 6(a), the intrinsic resistivity calculated with ERTA deviates from the one calculated by the iteration approach by less than 1%. Therefore, we will use the numerical results calculated with ERTA for the following discussions. The calculated intrinsic resistivity along the  $b$  axis of FM Gd between the two cases with and without SOC are compared in Fig. 6(b). We can see that the intrinsic resistivity with SOC is nearly 3 times greater than the one without SOC. Such a result verifies our anticipation that SOC enhances the intrinsic resistivity sizably.

We now concentrate on the contributions of electronic states around the K point and in the Fermi window to the

intrinsic conductivity since only these states are nontrivially changed by SOC. We learn from Eq. (7) that the factor  $f_{nk}(1 - f_{nk})$ , the relaxation time ( $\tau_{nk}$ ), as well as the squared velocity component along the electronic transport direction ( $v_{nk,x}^2$ ) within the Fermi window are relevant to the intrinsic conductivity. Therefore, it is significant to perform a detailed analysis on the change of these three quantities by SOC for the electronic states around the K point. This can help us to nail down the main source of the sizable increase of intrinsic resistivity by SOC. In so doing, in Fig. 7 we show the numerical results of these three quantities in the Fermi window, together with the local band structures around the K point. And the results with and without SOC are shown simultaneously for comparison. As one can see from Fig. 7(a), the band crossings in the absence of SOC are superseded by the local band gaps due to the presence of SOC. In more detail, let us look at such a change of band structure close to the Fermi level where the electronic states are tightly associated with the electronic transport property. As shown in Fig. 7(a), in the case without SOC, there are two band segments of minority spin which span the Fermi level with strong dispersion along M-K and K- $\Gamma$  lines, respectively. They are positioned by the two vertical gray strips throughout Fig. 7 where each of them intersects with a flat band of minority spin near the Fermi level. In the presence of SOC, these two band segments of strong dispersion disappear in the vicinity of the Fermi level. These states are pushed away from the Fermi level, due to the gap opening by SOC. Thus, they appear much farther away from the Fermi level, meanwhile, with spin mixing and much weaker dispersion. In view of that the strong dispersion means high velocity, the disappearance of these states near the Fermi level is presumably the main reason for the sizable increase of intrinsic resistivity by SOC as shown in Fig. 6(b). In addition, as seen from Fig. 7(a), for the states spanning the Fermi level elsewhere, SOC does not change notably the band structure therein except that one more flat band with strong spin mixing occurs around the K point and very close to the Fermi level. However, one should note that a flat band does not take part in the electronic transport process substantially.

Next, in Fig. 7(b) we show the electronic state resolved intrinsic conductivity, i.e.,  $\sigma_{nk}$  as defined in Eq. (7), along the  $b$  axis at 280 K. It is proportional to the product of the three quantities relevant to the intrinsic conductivity at a given temperature. From Fig. 7(b) we can see that only for those electronic states in the two gray vertical strips, the corresponding  $\sigma_{nk}$ 's show large discrepancy between the two cases with and without SOC. Hence, they are responsible for the sizable increase of the total intrinsic resistivity by SOC. In more detail, we can get such an impression from the numbers beside the black arrows in the figure which give the local maximal values of  $\sigma_{nk}$  in the two gray vertical strips of the two cases with and without SOC. In either of the two regions, such a maximum in the case without SOC is larger than that with SOC by almost two orders of magnitude. Therefore, in the following we will focus only on the two regions marked by the two gray vertical strips when exposing the individual feature of the three quantities relevant to the intrinsic conductivity. In Fig. 7(c) the quantity  $v_{nk,x}^2$  for those electronic states around the K point and in the Fermi window is shown. We can see readily that those states falling in the two gray vertical strips

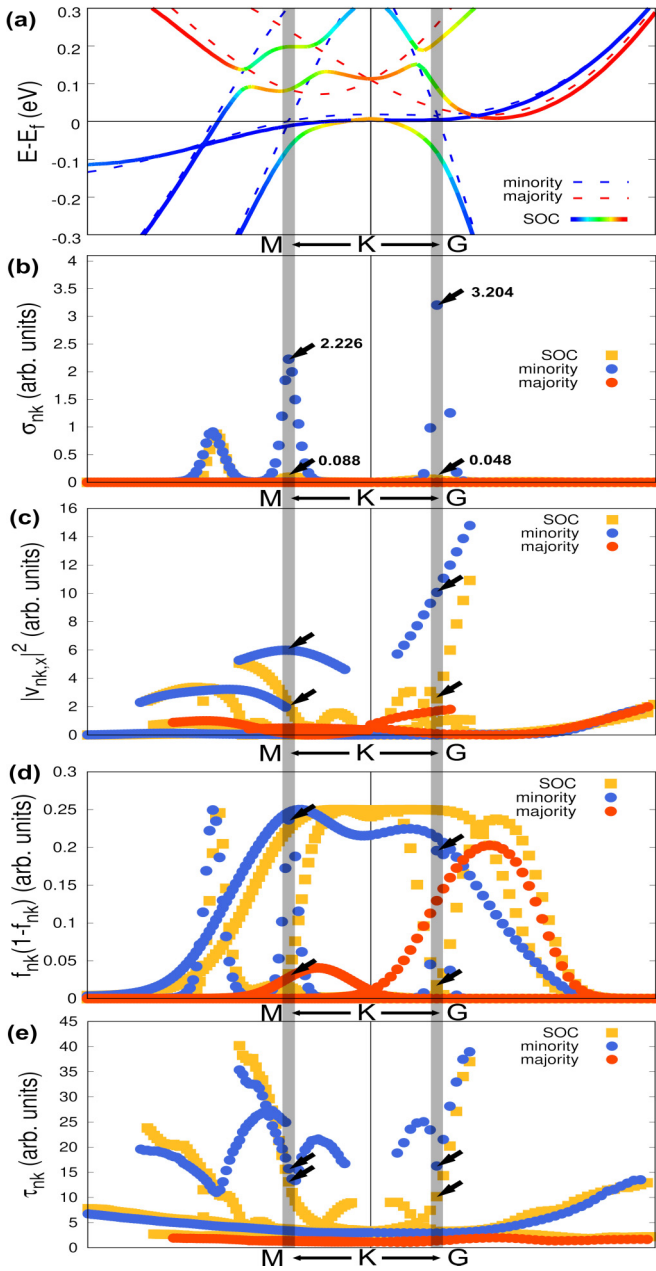


FIG. 7. (a) The electron band structures; (b) the electronic state resolved conductivity along  $b$  axis; (c) the factor  $f_{nk}(1 - f_{nk})$ ; (d) the square of electron band velocity component  $v_{nk,x}^2$  along  $b$  axis; and (e) the relaxation time  $\tau_{nk}$  around K points along M-K-G high-symmetry line in the cases with and without SOC. The temperature is set at 280 K for calculating the conductivity and relaxation time. Note that all quantities here are calculated within the Fermi window. The black arrows remind us of the difference between the typical values of the calculated quantities in the cases with and without SOC in the gray vertical strips.

have remarkable decrease in the squared velocity component, as SOC is switched on. In contrast,  $v_{nk,x}^2$ 's elsewhere as shown in Fig. 7(c) do not have such an appreciable variation if we pay attention only to those electronic states very close to the Fermi level. This result is consistent with the band structure shown in Fig. 7(a). To compare the relative importance of the electronic

states to the intrinsic resistivity, in Fig. 7(d) we plot the factor  $f_{nk}(1 - f_{nk})$  for those electronic states as shown in Fig. 7(a). We can see that scattered points (blue circles) in the two gray vertical strips correspond to the aforementioned band segments of minority spin with strong dispersion in the case without SOC. However, in the presence of SOC, such bands cannot display appreciable peaks in Fig. 7(d). This result is due to the fact that these bands are pushed largely away from the Fermi level due to the SOC effect. Therefore, they become less important to the intrinsic conductivity. In Fig. 7(e) the electronic relaxation times ( $\tau_{nk}$ ) are shown for the electronic states around the K point and in the Fermi window. We can see that the relaxation times of those states in the two gray vertical strips are reduced by the SOC effect, which means a stronger e-ph scattering and further the larger resistivity. However, such a decrease in relaxation time due to SOC is not as significant as the other two quantities shown in Figs. 7(c) and 7(d). From this result we can infer that the SOC cannot alter the e-ph interaction matrix element remarkably.

In short, we can now conclude that the main reason for the sizable increase of intrinsic resistivity by SOC is that the SOC opens gaps. As a result, the high-speed electrons close to the Fermi level in the case without SOC are pushed away from the Fermi level. Meanwhile, the band velocity is largely suppressed due to the band deformation by SOC. These two kinds of effects are combined to cause the sizable increase of the intrinsic resistivity.

Finally, we make a comparison between the calculated resistivity and the experimental result, which is presented in Fig. 8. First of all, we can find that when the SOC is taken into account, the calculated intrinsic resistivity increases remarkably, in comparison with the case without SOC, as has been shown in Fig. 6. In addition, such a case is independent of the electronic transport direction as seen from Figs. 8(a) and 8(b). However, we can also see that the intrinsic resistivity even with the SOC effect is still notably smaller than the experimental values of resistivity. This indicates that the resistivity arising from other scattering mechanisms cannot be disregarded even near the room temperature, such as that due to the spin fluctuation scattering as pointed out in previous work. Consulting Ref. [15], we obtain the value of the resistivity arising from spin fluctuation scattering. Then we add it to the intrinsic resistivity to get the final theoretical value of resistivity. From Fig. 8 we can find that such a theoretical result agrees with the experimental observation of the resistivity of FM Gd very well, much better than the previous theoretical result.

Thus far, our numerical results are wholly limited within the LDA method. Therefore, it is significant to have a look at the effect of SOC on the band structure of FM Gd beyond LDA before ending our work. In so doing, we calculate the band structure of FM Gd on the level of hybrid density functional, more specifically, by using HSE06 functional. The band structure around the Fermi energy and along the symmetric lines in the BZ is shown in Fig. 9. As one can see, only the band structure around the K point is modified by SOC nontrivially, like the case of LDA as shown in Fig. 7(a). By comparing the local band structures around the K point shown in Fig. 9(b) and Fig. 7(a), we can first see that the flat band in the vicinity of the Fermi energy observed previously in LDA

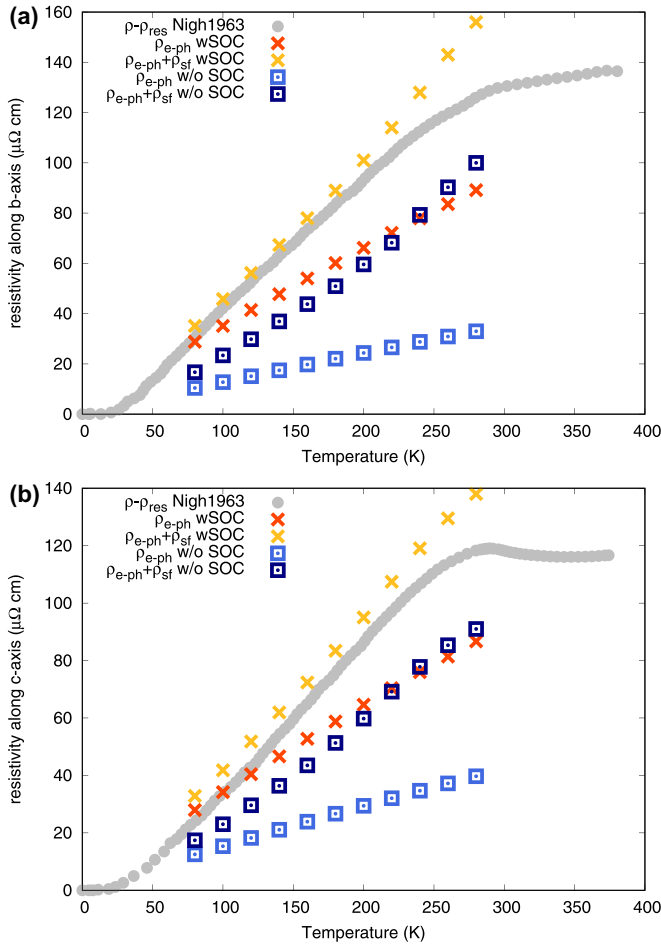


FIG. 8. The measured and calculated resistivity of FM Gd with SOC and without SOC (a) along  $b$  axis and (b) along  $c$  axis as a function of temperature. The measured resistivity shown as the gray circles has the residual resistivity subtracted as in Ref. [16] and the  $\rho_{sf}$  stands for the resistivity limited by the spin fluctuation calculated in Ref. [15].

disappears in Fig. 9(b). However, it does not matter to the resistivity since a flat band hardly contributes to the electronic transport. What is of importance in Fig. 9 is that two bands of spin minority with relatively high electronic velocities, which span the Fermi energy in the case without SOC as indicated by the two shaded regions in Fig. 9(b), are pushed away from the Fermi energy by the SOC effect. It bears a high analogy with the result of LDA band structure as shown in Fig. 7(a). Therefore, we can say that the band structure of the hybrid density functional supports our conclusion about the reason for the resistivity enhancement of FM Gd by the SOC effect drawn from the LDA method. Nonetheless, we cannot perform a further calculation about the intrinsic resistivity on the level of the hybrid density functional which is beyond the current applicability of the QE code. In contrast, within the LDA, the QE code provides us with a self-contained ability to perform a first-principles study on the intrinsic resistivity even for a heavy atomic material such as Gd. However, it is highly desirable to improve the ability to perform a first-principles calculation on the intrinsic resistivity of heavy atomic materials beyond LDA, such as hybrid density functionals or

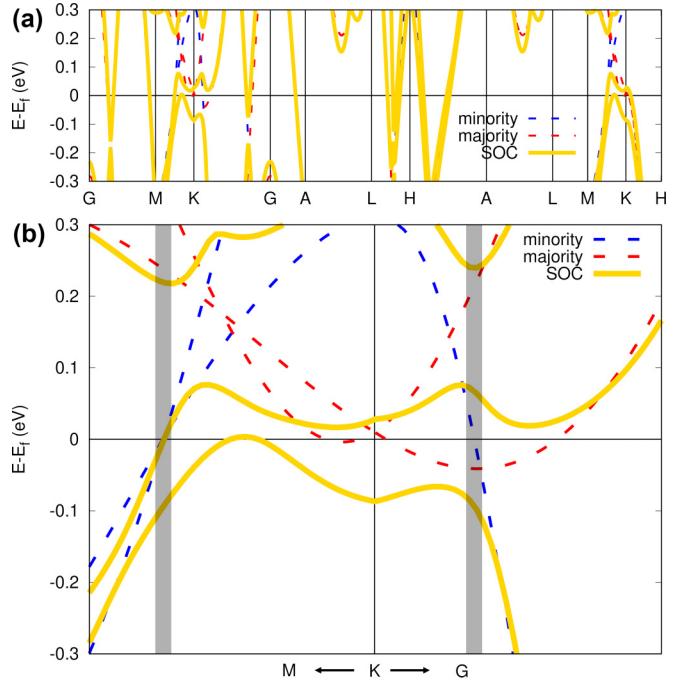


FIG. 9. (a) The electron band structure of FM Gd calculated with HSE06 functional. (b) The zoom-in band structure around K point in the BZ. The band structure with SOC is plotted as golden lines. The band structures without SOC are plotted as red and blue dashed lines for majority spin states and minority states, respectively. The  $\mathbf{k}$  and  $\mathbf{q}$  meshes in HSE06 calculation are all set to be  $6 \times 6 \times 6$ .

dynamical mean field theory. But it seems an arduous job in the near future.

#### IV. CONCLUSIONS

In summary, we studied the influence of the Hubbard  $U$  and SOC on the resistivity limited by e-ph scattering of FM Gd within the theoretical framework of the BTE by using DFT+ $U$  and DFPT+ $U$  approaches. We find that the Hubbard  $U$  has limited impact on the electronic and phononic band structures, e-ph scattering, and hence the intrinsic resistivity of FM Gd. The SOC effect, on the contrary, has a crucial impact on the electronic structures of Gd near the Fermi level and raises the intrinsic resistivity sizably compared with the one without SOC. By further analysis on the electronic band structure, electron velocity, and the electron relaxation time due to e-ph scattering, we find that the increase in the intrinsic resistivity arises from the SOC opened band gaps near the Fermi level around the K point in the BZ. More specifically, the band gap opening by SOC pushes some electronic states with high velocities, very close to the Fermi level in the case without SOC, away largely from the Fermi level. Consequently, the contributions of those electronic states to the intrinsic conductivity decrease dramatically. Then the calculated intrinsic resistivity in the presence of SOC increases by nearly 3 times over that without SOC. By further counting in the additional resistivity contributed from spin fluctuation scattering, our theoretical result of resistivity agrees very well with the experimental observation of resistivity of FM Gd as a function of temperature, which is much better than previous theoretical works.

## ACKNOWLEDGMENTS

This work was financially supported by the National Natural Science Foundation of China (Grants No. 12174145 and

No. 11774123) and the Natural Science Foundation of Jilin Province of China (Grant No. 20190201123jc). We thank the High Performance Computing Center of Jilin University for their computational resources.

- [1] W. E. Pickett, Electronic structure of the high-temperature oxide superconductors, *Rev. Mod. Phys.* **61**, 433 (1989).
- [2] N. F. Mott, The basis of the electron theory of metals, with special reference to the transition metals, *Proc. Phys. Soc. A* **62**, 416 (1949).
- [3] N. F. Mott, Metal-insulator transition, *Rev. Mod. Phys.* **40**, 677 (1968).
- [4] X.-L. Qi and S.-C. Zhang, Topological insulators and superconductors, *Rev. Mod. Phys.* **83**, 1057 (2011).
- [5] E. E. Schumacher and J. E. Harris, Investigation of the thermionic properties of the rare-earth elements, *J. Am. Chem. Soc.* **48**, 3108 (1926).
- [6] V. V. Vorob'ev, Y. N. Smirnov, and V. A. Finkel, Crystal structure of gadolinium at 120–370° K, *Sov. Phys. JETP* **22**, 1212 (1966).
- [7] R. M. Moon, W. C. Koehler, J. W. Cable, and H. R. Child, Distribution of magnetic moment in metallic gadolinium, *Phys. Rev. B* **5**, 997 (1972).
- [8] L. Oroszlány, A. Deák, E. Simon, S. Khmelevskiy, and L. Szunyogh, Magnetism of Gadolinium: A First-Principles Perspective, *Phys. Rev. Lett.* **115**, 096402 (2015).
- [9] B. Harmon, V. Antropov, A. Liechtenstein, I. Solovyev, and V. Anisimov, Calculation of magneto-optical properties for 4f systems: LSDA + Hubbard  $U$  results, *J. Phys. Chem. Solids* **56**, 1521 (1995).
- [10] R. F. Sabiryanov and S. S. Jaswal, Bulk and surface 4f states of Gd, *Phys. Rev. B* **55**, 4117 (1997).
- [11] A. B. Shick, A. I. Liechtenstein, and W. E. Pickett, Implementation of the LDA+ $U$  method using the full-potential linearized augmented plane-wave basis, *Phys. Rev. B* **60**, 10763 (1999).
- [12] P. Kurz, G. Bihlmayer, and S. Blügel, Magnetism and electronic structure of hcp Gd and the Gd(0001) surface, *J. Phys.: Condens. Matter* **14**, 6353 (2002).
- [13] M. Petersen, J. Hafner, and M. Marsman, Structural, electronic and magnetic properties of Gd investigated by DFT+ $U$  methods: Bulk, clean and H-covered (0001) surfaces, *J. Phys.: Condens. Matter* **18**, 7021 (2006).
- [14] A. Scheie, P. Laurell, P. A. McClarty, G. E. Granroth, M. B. Stone, R. Moessner, and S. E. Nagler, Dirac Magnons, Nodal Lines, and Nodal Plane in Elemental Gadolinium, *Phys. Rev. Lett.* **128**, 097201 (2022).
- [15] K. Chadova, S. Mankovsky, J. Minár, and H. Ebert, Impact of finite temperatures on the transport properties of Gd from first principles, *Phys. Rev. B* **95**, 125109 (2017).
- [16] H. E. Nigh, S. Legvold, and F. H. Spedding, Magnetization and electrical resistivity of gadolinium single crystals, *Phys. Rev.* **132**, 1092 (1963).
- [17] K. Maezawa, K. Mori, K. Sato, Y. Saito, and S. Wakabayashi, Electrical resistivity in gadolinium single crystal, *J. Phys. Soc. Jpn.* **43**, 1815 (1977).
- [18] J. K. Glasbrenner, K. D. Belashchenko, J. Kudrnovský, V. Drchal, S. Khmelevskiy, and I. Turek, First-principles study of spin-disorder resistivity of heavy rare-earth metals: Gd–Tm series, *Phys. Rev. B* **85**, 214405 (2012).
- [19] J. Kudrnovský, V. Drchal, I. Turek, S. Khmelevskiy, J. K. Glasbrenner, and K. D. Belashchenko, Spin-disorder resistivity of ferromagnetic metals from first principles: The disordered-local-moment approach, *Phys. Rev. B* **86**, 144423 (2012).
- [20] E. Francisco, M. A. Blanco, and G. Sanjurjo, Atomistic simulation of SrF<sub>2</sub> polymorphs, *Phys. Rev. B* **63**, 094107 (2001).
- [21] H. Ebert, S. Mankovsky, K. Chadova, S. Polesya, J. Minár, and D. Ködderitzsch, Calculating linear-response functions for finite temperatures on the basis of the alloy analogy model, *Phys. Rev. B* **91**, 165132 (2015).
- [22] S. Baroni, S. de Gironcoli, A. Dal Corso, and P. Giannozzi, Phonons and related crystal properties from density-functional perturbation theory, *Rev. Mod. Phys.* **73**, 515 (2001).
- [23] V. I. Anisimov, J. Zaanen, and O. K. Andersen, Band theory and Mott insulators: Hubbard  $U$  instead of Stoner  $I$ , *Phys. Rev. B* **44**, 943 (1991).
- [24] V. I. Anisimov, I. S. Elfimov, N. Hamada, and K. Terakura, Charge-ordered insulating state of Fe<sub>3</sub>O<sub>4</sub> from first-principles electronic structure calculations, *Phys. Rev. B* **54**, 4387 (1996).
- [25] V. I. Anisimov, F. Aryasetiawan, and A. I. Liechtenstein, First-principles calculations of the electronic structure and spectra of strongly correlated systems: The LDA + $U$  method, *J. Phys.: Condens. Matter* **9**, 767 (1997).
- [26] S. L. Dudarev, G. A. Botton, S. Y. Savrasov, C. J. Humphreys, and A. P. Sutton, Electron-energy-loss spectra and the structural stability of nickel oxide: An LSDA+ $U$  study, *Phys. Rev. B* **57**, 1505 (1998).
- [27] A. Floris, S. de Gironcoli, E. K. U. Gross, and M. Cococcioni, Vibrational properties of MnO and NiO from DFT+ $U$ -based density functional perturbation theory, *Phys. Rev. B* **84**, 161102(R) (2011).
- [28] A. Floris, I. Timrov, B. Himmetoglu, N. Marzari, S. de Gironcoli, and M. Cococcioni, Hubbard-corrected density functional perturbation theory with ultrasoft pseudopotentials, *Phys. Rev. B* **101**, 064305 (2020).
- [29] P. Giannozzi, S. Baroni, N. Bonini, M. Calandra, R. Car, C. Cavazzoni, D. Ceresoli, G. L. Chiarotti, M. Cococcioni, I. Dabo, A. Dal Corso, S. de Gironcoli, S. Fabris, G. Fratesi, R. Gebauer, U. Gerstmann, C. Gougoussis, A. Kokalj, M. Lazzeri, L. Martin-Samos *et al.*, Quantum Espresso: A modular and open-source software project for quantum simulations of materials, *J. Phys.: Condens. Matter* **21**, 395502 (2009).
- [30] P. Giannozzi, O. Andreussi, T. Brumme, O. Bunau, M. B. Nardelli, M. Calandra, R. Car, C. Cavazzoni, D. Ceresoli, M. Cococcioni, N. Colonna, I. Carnimeo, A. D. Corso, S. de Gironcoli, P. Delugas, R. A. DiStasio, A. Ferretti, A. Floris, G. Fratesi, G. Fugallo *et al.*, Advanced capabilities for materials modelling with Quantum ESPRESSO, *J. Phys.: Condens. Matter* **29**, 465901 (2017).

- [31] W. Li, Electrical transport limited by electron-phonon coupling from Boltzmann transport equation: An *ab initio* study of Si, Al, and MoS<sub>2</sub>, *Phys. Rev. B* **92**, 075405 (2015).
- [32] J.-J. Zhou and M. Bernardi, *Ab initio* electron mobility and polar phonon scattering in GaAs, *Phys. Rev. B* **94**, 201201(R) (2016).
- [33] J.-J. Zhou, O. Hellman, and M. Bernardi, Electron-Phonon Scattering in the Presence of Soft Modes and Electron Mobility in SrTiO<sub>3</sub> Perovskite from First Principles, *Phys. Rev. Lett.* **121**, 226603 (2018).
- [34] G. Pizzi, V. Vitale, R. Arita, S. Blügel, F. Freimuth, G. Géranton, M. Gibertini, D. Gresch, C. Johnson, T. Koretsune, J. Ibañez-Azpiroz, H. Lee, J.-M. Lihm, D. Marchand, A. Marrazzo, Y. Mokrousov, J. I. Mustafa, Y. Nohara, Y. Nomura, L. Paulatto *et al.*, Wannier90 as a community code: New features and applications, *J. Phys.: Condens. Matter* **32**, 165902 (2020).
- [35] J.-J. Zhou, J. Park, I.-T. Lu, I. Maliyov, X. Tong, and M. Bernardi, Perturbo: A software package for *ab initio* electron-phonon interactions, charge transport and ultrafast dynamics, *Comput. Phys. Commun.* **264**, 107970 (2021).
- [36] F. H. Spedding, A. H. Daane, and K. W. Herrmann, The crystal structures and lattice parameters of high-purity scandium, yttrium and the rare earth metals, *Acta Crystallogr.* **9**, 559 (1956).
- [37] L. W. Roeland, G. J. Cock, F. A. Muller, A. C. Moleman, K. A. McEwen, R. G. Jordan, and D. W. Jones, Conduction electron polarization of gadolinium metal, *J. Phys. F* **5**, L233 (1975).
- [38] I. Timrov, N. Marzari, and M. Cococcioni, Hubbard parameters from density-functional perturbation theory, *Phys. Rev. B* **98**, 085127 (2018).
- [39] I. Timrov, N. Marzari, and M. Cococcioni, Self-consistent Hubbard parameters from density-functional perturbation theory in the ultrasoft and projector-augmented wave formulations, *Phys. Rev. B* **103**, 045141 (2021).